Journal of Neuroimaging
Official Journal of the American Society of Neuroimaging

# The Role of Multimodal MRI in Mild Cognitive Impairment and Alzheimer's Disease



| | |
|---|---|
| Journal: | *Journal of Neuroimaging* |
| Manuscript ID | JON-21-6284.R2 |
| Wiley - Manuscript type: | Experimental Laboratory Research |
| Date Submitted by the Author: | 28-Sep-2021 |
| Complete List of Authors: | Knudsen, Laust; Syddansk Universitet,<br>Gazerani, Parisa ; Aalborg Universitet<br>Michel, Tanja Maria ; Syddansk Universitet<br>Seyedi Vafaee, Manouchehr ; Syddansk Universitet |
| Keywords: | Alzheimer's disease, Mild cognitive impairment, magnetic resonance imaging, support vector machine, clinical assessment |
| Subject Area: | Alzheimer-s Disease < Neurodegenerative Diseases < Diseases < NEUROIMAGING, Magnetic Resonance Imaging (MRI) < Magnetic Resonance (MR) < Imaging Techniques < NEUROIMAGING, Diffusion Tensor Imaging (DTI) < Magnetic Resonance (MR) < Imaging Techniques < NEUROIMAGING |
| | |

**Title:** The Role of Multimodal MRI in Mild Cognitive Impairment and Alzheimer's Disease

**Authors:** Laust Vind Knudsen[1]. Parisa Gazerani[2]. Tanja Maria Sheldrick-Michel[1]. Manouchehr Seyedi Vafaee[1].

[1] Research Unit for Psychiatry, Odense University Hospital, Odense, Denmark

[2] Department of Health Science and Technology, Faculty of Medicine, Aalborg University, Aalborg, Denmark

**Corresponding author**: Laust Vind Knudsen. J.B. Winslowsvej 20, 5000 Odense C, DK. laustvindknudsen@gmail.com. +4526234329.

**Author order:** Laust, V, Knudsen. Parisa, Gazerani. Tanja Maria Sheldrick-Michel. Manouchehr, S. Vafaee.

**Institutional affiliation:** Manouchehr Seyedi Vafaee, psychiatry syddansk universitet, 5000 Odense C, DK. Parisa Gazerani, institute of medicin and health technology, 9220 Aalborg, DK. Tanja Maria Michel, psychiatry syddansk universitet, 5000 Odense C, DK.

**Keyword:** Alzheimer's disease, mild cognitive impairment, magnetic resonance imaging, support vector machine, clinical assessment.

**Funding**: none

## Abstract

**Background and Purpose**: Mild cognitive impairment (MCI) is a prodromal stage of Alzheimer's Disease (AD), where neurodegeneration is not as considerable, thereby potentially increasing the effect of treatments. Therefore, highly sensitive and specific classification of subjects with MCI is necessary, where various MRI modalities have displayed promise.

**Methods**: Structural, diffusion and resting state (RS) functional MRI analysis were performed on the AD (n=26), MCI (n=5) and healthy control (HC) (n=14) group. Structural analysis was performed via voxel-based morphometry (VBM) and volumetric subcortical segmentation analysis. Fractional anisotropy and mean diffusivity were estimated during the diffusion analysis. RS analysis investigated seed-based functional connectivity. Classification via support vector machine was performed to evaluate which MRI modality most accurately differentiated the groups. Multiple linear regression was conducted to evaluate the MRI modalities correlation with clinical assessment scores.

**Results**: Classification of MCI and N displayed highest accuracy based on diffusion MRI, which besides demonstrated high correlation with clinical scores. Classification was equally accurate in AD, when using VBM or diffusion tensor imaging measures. Yet, more variance was explained by VBM measures in the clinical assessment scores of the AD group.

**Conclusions**: This study highlights the potential of diffusion MRI in differentiating MCI from HC and AD. However, the results need to be interpreted with caution as sample size and artifacts in the MRI data probably influenced the results.

## Introduction

The increased lifespan of modern society, amplifies the risk of age-related diseases such as dementia.[1] In 2015 alone around 47 million people worldwide have been affected by those. It is expected to affect 132 million in 2050.[2] The most common form of dementia is Alzheimer's disease (AD) with 60-70% of all dementia cases.[3] AD has a destructive impact on cognitive abilities, especially affecting memory function.[4] The precise neurobiological mechanisms for the brain damage remain to be elucidated,[5] but implicates amyloid-beta (Aβ) deposition and hyperphosphorylated tau-containing neurofibrillary tangles (NFT), that initiate synapse and neuronal damage and loss.[4,5] Molecular imaging as positron emission tomography (PET) have contributed greatly to the understanding and diagnosis of AD. Where associations between AD severity and Aβ deposition,[6] NFT quantity,[7] and glucose hypometabolism.[8] However, the invasive nature and comparatively high cost of PET, has increased the popularity of MRI as a imaging tool for exploring biomarkers.[9] Structural MRI (sMRI) is exploited for assessment of grey matter volume (GMV) difference,[10] which have identified atrophy of the medial temporal lobe (MTL) as a hallmark in AD patients.[11] MTL atrophy is not as extensive in MCI patients, but advances with disease severity.[11] Diffusion MRI (dMRI) involves the Brownian motion of water molecules,[12] that enables the white matter integrity (WMI) to be evaluated, which is influenced by axon density, directional homogeneity of axons, axon membrane integrity, myelination, and inflammation as gliosis.[12] Both MCI and AD patients display decreased WMI,[13,14] with further extensive WMI decrease exhibited later in the AD continuum.[13,14] Functional MRI (fMRI), which exploits Blood-Oxygen-Level-Dependent signal,[15] can be applied to investigate the temporal correlation of brain activity, referred to as functional connectivity (FC).[16] MCI patients exhibits abnormal FC within default mode network (DMN) structures, such as the posterior cingulate cortex (PCC), angular gyrus, parahippocampal gyrus, fusiform gyrus and middle temporal gyri.[16] These tendencies are similarly displayed in AD patients, but with severe abnormalities.[17] Therefore, comparisons of multi-modal

MRI data, using sMRI, dMRI and fMRI, from healthy controls (HC), MCI and AD patients, could elicit group differences and thereby propose potential biomarkers for the differentiation and diagnosis of MCI patients. The study was designed to perform a multi-modal MRI investigation, to breed biomarkers and examine their relationship with cognitive assessments and their usefulness in classification using support vector machine (SVM). We hypothesized that GMV, WMI and FC would decrease with progression in the AD continuum.

## Methods

*Participants*. In total we studied 45 right-handed subjects, who were diagnosed by neurologists at the Tiantan Hospital in Beijing. The group was comprised of 26 AD and 5 MCI patients and 14 healthy subjects. There were no significant differences in mean age among the groups, i.e., mean ± standard deviation for AD (64.5 ± 6.51 years), MCI (63.4 ± 6.89 years), HC (62.7 ± 3.54 years).

*MRI acquisition*. All MRI data were acquired using a 3.0 T Phillips T Ingenia CX scanner (Philips, Eindhoven, Netherlands) at Tiantan Hospital in Beijing, China. The sagittal T1-weighted (T1W) MR images were performed by a three-dimensional turbo fast echo acquisition at subsequent parameters; Repetition time (TR) = 6.6 ms, echo time (TE) = 3 ms, flip angle = 8◦, field of view (FOV) = 256 x 256 mm, matrix = 256 x 256, number of slices = 196, slice thickness = 1mm, scan time = 3.53 min. The diffusion tensor images were performed by a spin echo diffusion-weighted echo planar imaging sequence with the following parameters: 6 diffusion directions at b = 1000 s/mm$^2$ for each direction, TR = 4 s, TE = 86 ms, flip angle = 90◦, matrix size = 85 x 85, FOV 193 x 193 mm, slice thickness = 2.5 mm, scan time = 6.2 min. The functional data were performed via an echo planar imaging sequence with the following parameters: TR = 2 s, TE=30 ms, flip angle = 78◦, matrix size: 62 x 62, FOV:186 x 186 mm, slice thickness = 4 mm, scan time = 5.97 min. All MRI modalities were initially in Digital Imaging and Communication in Medicine format, which were transformed into Neuroimaging Informatic Technology Initiative format, via the dcm2niix command.[18]

*Structural MRI preprocessing.* The T1W images were preprocessed via FSL_anat,[19] where the images were reoriented to the Montreal Neurological Institute (MNI) standard image MNI-152, the neck was removed, and bias-field correction was performed, to correct for intensity inhomogeneities.[20]

*Structural MRI analysis via Voxel-based morphometry.* VBM was utilized as part of the structural analysis.[19] To optimize registration, a study-specific template was generated, based on 15 subjects, 5 from each group.[21] For inference, non-parametric testing using 5000 permutations was performed.[22] For test-statistic threshold-free cluster enhancement (TFCE) was selected.[23] Furthermore, multiple comparison correction (MCC) via family-wise error (FWE), was performed, as part of the statistical analysis via randomise and TFCE. Age and gender were used as covariates, to remove their impact on volumetric characteristics.[24] Regions-of-interests (ROIs) were extracted from the overlap, minimum 60% overlap, between the significant statistical maps and the Harvard-Oxford Subcortical Structural Atlas and Harvard-Oxford Cortical Structural Atlas.[25]

*Subcortical segmentation analysis.* Subcortical segmentation was performed via FMRIB´s Integrated Registration and Segmentation Tool (FIRST).[26] Seven structures were selected (left and right amygdala, hippocampus, putamen, left and right thalamus), selected based on indication of atrophy in the VBM analysis. The subcortical volumes in native space, were corrected for head size via the V-scaling factor (1.44 ± 0.13) produced by Structural Image Evaluation, using Normalization, of Atrophy.[27] To test for significant group differences on the head size corrected subcortical volumes, analysis of covariance (ANCOVA) was executed in SPSS (SPSS, Version 25). ANCOVA enabled removal of age and gender effects impact on volumetric characteristics.[24] Subsequently, post-hoc tests with Bonferroni MCC (0.05/18) were applied on the significant ANCOVA ($p<0.05$) results.

*Diffusion MRI preprocessing.* The images were corrected for eddy currents and motion artifacts via FSLs Eddy_correct.[27] DTIFIT were used together with the diffusion images, mask, bvec and bval file to fit a diffusion tensor model at each voxel, thereby generating images with a diffusion measure as contrast.[28] Fractional anisotropy (FA) and mean diffusivity (MD) were selected as diffusion contrasts.

*Diffusion MRI analysis*. Tract-Based Spatial Statistics (TBSS) were used for the diffusion analysis. Where the most typical image, i.e., the image that demands the least warping to align with the other images was selected, to improve registration. The TBSS procedure generated an FA image, while the MD image was generated via tbss_non_FA.[27] Subsequently, the FA and MD images were used in statistical testing using permutation based non-parametric testing with MCC, FWE and TFCE with 2-dimensional optimization.[27] Age and gender were used as covariates, as these influence diffusion measures.[29] ROIs were selected based on the overlap, minimum 60% overlap, between the MCC statistical map and the International Consortium for Brain Mapping-DTI-81 white-matter labels atlas[30] as well as the Johns Hopkins University White Matter Tractography Atlas.[31]



*fMRI preprocessing.* The images were preprocessed via FEAT.[32] The first five volumes were removed, increasing probability of obtained magnetic equilibrium.[33] Furthermore, MCFLIRT was selected for registration and motion correction together with spatial smoothing of 6 mm.[19] These selections were based on best practice for the following preprocessing via Independent Component Analysis - Automatic Removal of Motion Artifacts (ICA-AROMA).[34] Initially the data was decomposed into independent components (ICs) by FSLs Multivariate Exploratory Linear Optimized Decomposition into Independent Components.[35] Next ICA-AROMA classified these ICs into motion/noise or neuronal signals, based on the ICs inherent high-frequency content, correlation with realignments parameters, edge fraction and CSF fraction. ICs classified as movement associated were regressed of the of data.[34] Afterwards, WM and CSF segmentations were utilized to remove WM and CSF signal from the image. Lastly the denoised images were high-passed filtered (<0.01 Hz), to increase sensitivity and transformed to MNI space.[34]

*Seed-based fMRI analysis*. The PCC, Precuneus Cortex (PC) and the Hippocampus were selected as seeds and a mask of these structures in MNI space were created. The selected structures were selected as they displayed atrophy in the VBM analysis and part of the DMN. Next the timeseries was extracted from the structure masks and first-level FEAT analysis was performed and subsequently higher-level analysis were executed.[19] Conclusively, permutation based non-parametric testing was performed to test for group differences. The MNI152_T1_2mm template was applied as a mask and TFCE were utilized as test statistic via FSLs randomise with FWE MCC.[19] Gender and age were use as covariate, since these influences FC.[36]

*Support vector machine*. To investigate which MRI modalities were advantageous in classification purposes, support vector machine was implemented. The SVM analysis was conducted in R (R Core Team, 2014) utilizing the caret package.[37] Initially, features were demeaned and divided by the standard deviation, to avoid large-valued features to dominate.[38] Feature selection was performed via Least Absolute Shrinkage and Selection Operator regression where the optimal tuning parameter $\lambda$ was found via cross validation.[39] The data were split into training and test set, 80% and 20% respectively, and cross-validation was performed to estimate the optimal tuning parameters. The SVM model were trained to classify the groups (AD, MCI, or HC). This was done with a polynomial kernel and receiver operating characteristic curve was selected as the metric for estimating the best tuning parameters for the SVM. Subsequently, the SVM model was tested on the test data set. This was performed on two groups at a time, using different combinations of MRI modality, to explore which would classify the groups most accurately.

*Multiple linear regression*. Multiple linear regression (MLR) was performed to investigate the groups correlation and variance between Mini-Mental State Examination/Montreal Cognitive Assessment (MMSE/MoCA) score, based on the correlation coefficient and adjusted R2. Adjusted R2 was selected instead of $R^2$, as $R^2$ increases as a function of included variables, while adjusted R2 only increases with model improvement, giving a less biased outcome.[40] The procedure was performed in SPSS.



**Results**

*VBM analysis*. The VBM analysis revealed significant GMV differences in the precuneus cortex (PC) between MCI and AD, thereby implying higher GMV in MCI compared to AD, see table 1 and figure 1. Furthermore, widespread GMV differences were displayed between HC and AD, indicating higher GMV in HCs. see table 1 and figure 1.

Figure 1: The statistically significant results from the voxel-based morphometry analysis, highlighted in blue on top of the Montreal Neurological Institute-152 1mm template. The top image demonstrates the significant results of t-test Mild cognitive impairment>Alzheimer's disease. The bottom image depicts the significant results from the t-test Healthy control>Alzheimer's disease.

*FIRST analysis.* The subcortical volumetric analysis demonstrated significant difference in AD compared to HC in the left and right hippocampus and putamen, the right thalamus, and the left amygdala, after Bonferroni correction, see table 2. However, no significant differences were found when comparing MCI and AD after Bonferroni correction.

*DTI analysis.* The DTI analysis displayed significantly higher FA in HC compared to AD, which involved a variety of WM tracts, that are illustrated in table 3 (HC>AD) and figure 2. No differences were found when comparing MCI and AD nor MCI and HC. However, using MD as diffusion measure, significantly higher MD was found in MCI compared to HC, see table 2 and figure 2. Additionally, more widespread significant MD difference was found between AD and HC, as illustrated in table 3 and figure 2. Nonetheless, no significant differences were apparent between MCI and AD.

Figure 2: Significant group differences in fractional anisotropy (FA) and mean diffusivity (MD) are highlighted in blue, on top of the FSL_HCP1065_FA_1mm template. The top image illustrates FA difference between healthy controls>Alzheimer's disease, while the middle image exemplifies the difference in MD between mild cognitive impaired>healthy controls. The bottom image demonstrates the MD difference between healthy controls<Alzheimer's disease. Furthermore, the WM tracts overlapping with the statistical map is reported. Corpus Callosum body (CCB). Corpus Callosum genu (CCG). Corpus Callosum splenium (CCS). Anterior Corona Radiata (ACR). Superior Corona Radiata (SCR). External Capsule (EC). Cingulum Hippocampus (CH). Forceps Minor (FM). Inferior Fronto-Occipital Fasciculus (IFOF). Inferior Longitudinal Fasciculus (ILF). Anterior Thalamic Radiation (ATR). Posterior Corona Radiata (PCR).

*Resting state analysis*. The RS fMRI analysis yielded one minor significant result, which occurred between the PCC and Anterior Cingulate Cortex (ACC). This reflects a lower degree of coactivation between the PCC and part of the ACC in AD compared to HC. The cluster located in the ACC contained 126 voxels, with the peak voxel value located in the MNI coordinate x 10, y 32, z -8. No significant difference was found between the groups PCO.

*Support vector machine classification*. The classification results from the SVM are illustrated in table 4. The results illustrate a that DTI features were advantageous in classifying MCI from HC, compared to VBM and RS features. Further highlighted by the multi-modal model being primary consisting of DTI measures. In classification of AD and MCI, the multi-modal, DTI and VBM model performed equivalent. However, no model was capable of classifying MCI from AD, illustrated by the specificity being zero. Classification of AD vs HC displayed 100% accuracy when based on multi-modal or DTI, while VBM exhibited an accuracy of 86%. Summarized, DTI measures performed with higher accuracy, than any other single modality.

*Multiple linear regression*. The MLR results illustrated in table 5, indicates that MMSE/MoCA scores in the AD group, are correlated to a higher degree with DTI than VBM variables. Oppositely, VBM variables explains more variance than DTI variables, as illustrated in the top two rows of table 5. In the MCI group the DTI variables are correlated to a higher degree and explains more variance than VBM variables. In the HC group DTI appears more correlated and explains more variance than the VBM results. Additionally, it appears that VBM explains substantially more variance in MMSE than in MoCA scores, respectively 80% and 46% as seen in row six of table 5. No significant difference was apparent between correlations.

## Discussion

*Structural data*. The VBM results showed significant GM atrophy in AD compared to HC, with atrophy manifested in MTL structures, as hippocampus and the PHA, which supports existing evidence.[11,41] Presumably because this region is the first affected by NFTs and Aβ plaques in the AD continuum.[4] The VBM results were supported by the FIRST results, which likewise indicated atrophy of hippocampus in AD patients. Significant differences were displayed in the PC between

MCI and AD in the VBM analysis, while no significant differences were evident in the FIRST analysis after MCC. Positive correlations with MMSE/MoCA score were present in the AD group, which follows existing literature.[41] Illustrating a relationship between decreasing GMV and cognitive function. In summary, the structural analysis of GMV is sensitive between AD and HC, while difference between MCI and AD/HC was less apparent, indicating less sensitivity to GMV differences.

*DTI data*. FA displayed positives correlation with MMSE/MoCA scores in MCI and AD. Specifically, high correlation was found in the right Inferior Fronto-Occipital Fasciculus (IFOF), bilateral Superior Longitudinal Fasciculus (SLF) and Anterior Corona Radiata, which are associated with decreased memory function.[42] The negative correlations between MD and MMSE/MoCA score in AD and MCI, illustrate the relationship between WMI and cognition.[13] Interestingly, the MD differences between MCI and HC were primarily located in the left hemisphere (seven vs. three). This characteristic indicates inefficient communication of the left hemisphere.[43] The MD differences between AD and HC were widespread and included tracts as anterior thalamic radiation, forceps minor, forceps major, cingulum hippocampus, IFOF, SLF, inferior longitudinal fasciculus and Corpus Callosum, which are associated with early affected GM in the AD continuum, such as the Hippocampus, middle temporal gyrus and PCC.[42] These results thereby display an association with known AD pathology.[44] MD appeared more sensitive than FA, as it differentiated MCI and HC, which has been advocated previously.[45] As FA and MD are influenced by numerous factors, the interpretation of whether this is caused by demyelination, axonal density loss, membrane dysfunction, intracellular organelles or inflammation is enigmatic.[12] WMI reduction has been presumed to be instigated because of GM atrophy through Wallerian degeneration,[44] yet some WM damages may occur independently.[46,47] No significant differences were found between MCI and HC in the structural analysis, while differences were apparent in the DTI analysis. This might insinuate that WM damage could have occurred independently of GM atrophy, as supported previously,[48] or perchance that DTI measures are more sensitive in MCI.[48,49] However, this must be interpreted carefully, due to low sample size. Regardless of the underlying cause, in summary MD evidenced more sensitive than FA, and WMI appeared to worsen as patients were located later in the AD continuum.

*Resting state data*. The RS analysis only displayed significantly lower FC between the PCC and ACC in AD compared to HC, simulating previous findings,[17,50] and which is linked to memory performance.[51] Generally, decreased FC has been reported in both MCI and AD within the DMN, especially in the nodes of the DMN as PC, PCC and prefrontal cortex.[17] The PCC and ACC are involved in episodic memory processes, with decreased FC being linked to early episodic memory deficits in MCI and AD.[52]

*Support vector machine classification*. The SVM classified subjects from the MCI and HC group more accurately, when based on DTI features, compared to VBM features. Thereby indicating DTI as a sensitive measure for differentiating MCI and HC.[49] However, when classifying MCI and AD the SVM performed equally accurate, based upon DTI or VBM features. This result coincides with the consensus that both VBM and DTI features are sensitive in differentiating MCI and AD.[53] Surprisingly, DTI features displayed higher accuracy when classifying AD from HC, than VBM. Generally, VBM features are considered very sensitive in this manner,[41,53] and has been considered slightly more accurate than DTI.[53] However, evidently 11% of AD patients do not display GM atrophy,[54] which could explain the advantages of DTI. The multi-modality SVM did not display higher accuracies, although it is usually advantageous compared to single modality SVM.[53] However, due to the low power, these classification measures and sensitivity should be interpreted with caution, and further examinations should be performed, to assess whether DTI features truly are superior in classification purposes.

*Multiple linear regression*. The MLR showed high correlation between DTI and VBM measures and MMSE/MoCA scores, resembling the existing literature.[49] VBM explained more variance than DTI in AD, supporting the perception that GM atrophy drives the cognitive decline in AD.[4,44] DTI displayed stronger correlation and variance explained in MCI than VBM, potentially indicating decreased WMI as primus motor in cognitive impairment. Coinciding with evidence of Aβ affecting WM earlier, causing decreased WMI before GM atrophy.[47] The VBM measures explained more of the variance of MMSE scores in the HC group, while DTI explained more of the variance in MoCA scores of the N group. This confusing result could be instigated by the different nature of the MMSE and MoCA tests, as MoCA is aimed specifically for MCI subjects.

*Sample size.* The low sample size due to the pandemic, especially in the MCI group, triggers a high risk of false negatives, false positives and that results are caused by sampling variability.[55] The sample size is inadequate, which further influences the SVM analysis, as the group sizes should be of equal size, and feature quantity should not be of higher magnitude than subjects.[56] Therefore, the models including the MCI group were either optimally trained or tested. Additionally, the numerous variables and low sample size, included in the linear regression probably inflated the correlation coefficient and to a lower degree the adjusted-$R^2$.[40] In summary, the results of the study, especially involving the MCI group, should be interpreted with caution and doesn't allow for generalization.

*Distortion correction of DTI and fMRI data*. The spin-echo-planar imaging sequence used in diffusion imaging is cursed by hypersensitivity to off-resonance induced distortions, caused by low bandwidth of the phase-encoding direction.[57] Similar inherent distortions occur in fMRI data. Acquiring a fieldmap or an image with two different phase encoding directions,[57] would have enabled distortion correction. This would have improved registration, reduced between-subject variability in distortions and increased robustness and sensitivity.[57]

*Conclusion.* The results reveal higher sensitivity of DTI in differentiating MCI from HC and AD, which displayed stronger correlation with the clinical assessment scores. DTI and VBM seemed comparably sensitive in AD, as both measures were substantially progressed in AD compared to MCI and HC, although VBM explained more of the variance in clinical assessment scores in the AD group compared to DTI. Considering the limitations of this study, it must be interpreted cautiously. Increasing sample size and distortion correction of DTI and fMRI would increase reliability and validity. Therefore, a sharp conclusion cannot be made, and further investigation of DTI as an MCI diagnosis method needs to be performed. The study could however present that DTI appeared favorable in differentiating MCI, while DTI and VBM both seem suitable for differentiation of AD.

**Acknowledgments and Disclosure**

Initially I would like to express my sincere gratitude towards Kong Yazhuo for accepting me into his laboratory and tutoring me during the thesis process. Additional gratitude is sent towards Parisa Gazerani, for her diligent work with feedback and written materials. Additional appreciation is sent towards Manouchehr and Tanja, for their help with converting my thesis into an article. Subsequently great thankfulness is projected towards the Tiantan Image Research Center in Beijing, for allowing this article to be produced.

The author has no conflict of interest to disclose.

## References

1. Cao Q, Tan CC, Xu W, Hu H, Cao XP, Dong Q, et al. The prevalence of dementia: a systematic review and meta-analysis. J Alzheimers Dis 2020;73:1157–66.
2. Prince MJ, Wu F, Guo Y, et al. The burden of disease in older people and implications for health policy and practice. Lancet 2015;385:549–62.
3. Kalaria RN, Maestre GE, Arizaga R, et al. Alzheimer's disease and vascular dementia in developing countries: prevalence, management, and risk factors. Lancet Neurol 2008;7:812–26.
4. Raskin J, Cummings J, Hardy J, Schuh K, Dean R. Neurobiology of Alzheimer's disease: integrated molecular, physiological, anatomical, biomarker, and cognitive dimensions. Curr Alzheimer Res 2015;12:712–22.
5. De Strooper B, Karran E. The cellular phase of alzheimer's disease. Cell 2016;164:603–15.
6. Näslund J, Haroutunian V, Mohs R, et al. Correlation between elevated levels of amyloid β-peptide in the brain and cognitive decline. J Am Med Assoc 2000;283:1571–7.
7. Berg L, McKeel DW, Miller JP, et al. Clinicopathologic studies in cognitively healthy aging and Alzheimer disease. Arch Neurol 1998;55:326-27
8. Eliassen CF, Reinvang I, Selnes P, Grambaite R, Fladby T, Hessen E. Biomarkers in subtypes of mild cognitive impairment and subjective cognitive decline. Brain Behav 2017;7:3–9.
9. Hansson O, Lehmann S, Otto M, Zetterberg H, Lewczuk P. Advantages and disadvantages of the use of the CSF Amyloid β (Aβ) 42/40 ratio in the diagnosis of Alzheimer's disease. Alzheimers Res Ther 2019;11:1–15.
10. Ashburner J, Friston KJ. Voxel-based morphometry - The methods. Neuroimage

2000;11:805–21.

11. Frisoni GB, Fox NC, Jack CR, Scheltens P, Thompson PM. The clinical use of structural MRI in Alzheimer disease. Nat Rev Neurol 2010;6:67–77.

12. Beaulieu C. The basis of anisotropic water diffusion in the nervous system - A technical review. NMR Biomed 2002;15:435–55.

13. Yu J, Lam CLM, Lee TMC. White matter microstructural abnormalities in amnestic mild cognitive impairment: A meta-analysis of whole-brain and ROI-based studies. Neurosci Biobehav Rev 2017;83:405–16.

14. Mayo CD, Mazerolle EL, Ritchie L, Fisk JD, Gawryluk JR. Longitudinal changes in microstructural white matter metrics in Alzheimer’s disease. NeuroImage Clin 2017;13:330–8.

15. Devor A, Sakadžić S, Saisan PA, et al. “Overshoot” of O2 is required to maintain baseline tissue oxygenation at locations distal to blood vessels. J Neurosci 2011;31:13676–81.

16. Greicius MD, Supekar K, Menon V, Dougherty RF. Resting-state functional connectivity reflects structural connectivity in the default mode network. Cereb Cortex 2009;19:72–8.

17. Lau WKW, Leung MK, Lee TMC, Law ACK. Resting-state abnormalities in amnestic mild cognitive impairment: a meta-analysis. Transl Psychiatry 2016;6:1-2.

18. Li X, Morgan PS, Ashburner J, Smith J, Rorden C. The first step for neuroimaging data analysis: DICOM to NIfTI conversion. J Neurosci Methods 2010;264:47–56.

19. Smith SM, Jenkinson M, Woolrich MW, et al. Advances in functional and structural MR image analysis and implementation as FSL. Neuroimage 2004;23:208–19.

20. Juntu J, Sijbers J, Dyck D, Gielen J. Bias fieldcorrection for MRI images. Presented at the 4th International Conference on Computer Recognition Systems CORES; May 22-22, 2005; Rydzyna.

21. Mechelli A, Price C, Friston K, Ashburner J. Voxel-based morphometry of the human Brain:

methods and applications. Curr Med Imaging Rev 2005;1:105–13.

22. Winkler AM, Ridgway GR, Webster MA, Smith SM, Nichols TE. Permutation inference for the general linear model. Neuroimage 2014;92:381–97.

23. Smith SM, Nichols TE. Threshold-free cluster enhancement: Addressing problems of smoothing, threshold dependence and localisation in cluster inference. Neuroimage 2009;44:83–98.

24. Sowell ER, Peterson BS, Kan E, et al. Sex differences in cortical thickness mapped in 176 healthy individuals between 7 and 87 years of age. Cereb Cortex 2007;17:1550–60.

25. Desikan RS, Ségonne F, Fischl B, et al. An automated labeling system for subdividing the human cerebral cortex on MRI scans into gyral based regions of interest. Neuroimage 2006;31:968–80.

26. Patenaude B, Smith SM, Kennedy DN, Jenkinson M. A Bayesian model of shape and appearance for subcortical brain segmentation. Neuroimage 2011;56:907–22.

27. Smith SM, Jenkinson M, Johansen-Berg H, et al. Tract-based spatial statistics: Voxelwise analysis of multi-subject diffusion data. Neuroimage 2006;31:1487–505.

28. Behrens TEJ, Berg HJ, Jbabdi S, Rushworth MFS, Woolrich MW. Probabilistic diffusion tractography with multiple fibre orientations: What can we gain? Neuroimage 2007;34:144–55.

29. Kanaan RA, Chaddock C, Allin M, et al. Gender influence on white matter microstructure: A tract-based spatial statistics analysis. PLoS One 2014;9:1–6.

30. Dimitrova N, Zamudio JR, Jong RM, et al. Tract probability maps in stereotaxic spaces: analyses of white matter anatomy and tract-specific quantification. Neuroimage 2008;32:736–40.

31. Susumu M, Setsu W, Lidia, M N-P, Peter, C MVZ. MRI atlas of human white matter. Concepts Magn Reson Part A Bridg Educ Res 2006;28:180–1

32. Salmond CH, Ashburner J, Vargha-Khadem F, Connelly A, Gadian DG, Friston KJ. Distributional assumptions in voxel-based morphometry. Neuroimage 2002;17:1027–30.

33. Smith SM, Nichols TE. Threshold-free cluster enhancement: Addressing problems of smoothing, threshold dependence and localisation in cluster inference. Neuroimage 2009;44:83–98.

34. Pruim RHR, Mennes M. Rooij DV, Llera A, Buitelaar JK, Beckmann CF. ICA-AROMA: A robust ICA-based strategy for removing motion artifacts from fMRI data. Neuroimage 2015;112:267–77.

35. Christian, F B, Stephen, M S. Probabilistic independent component analysis for functional magnetic resonance imaging. Handb Clin Neurol 2004;174:265–75.

36. Sie J-H, Chen Y-H, Shiau Y-H, Chu W-C. Gender- and age-specific differences in resting-state functional connectivity of the central autonomic network in adulthood. Front Hum Neurosci 2019;13:1–13.

37. Kuhn M. Building predictive models in R using the caret package. J Stat Softw 2008;28:1–26.

38. Sidey-Gibbons JAM, Sidey-Gibbons CJ. Machine learning in medicine: a practical introduction. BMC Med Res Methodol 2019;19:1–18.

39. Tishbirani R. Regression shrinkage and selection via the Lasso. J R Stat Soc Series B Stat Methodol 1996:34;267–88.

40. Akossou AYJ, Palm R. Impact of data structure on the estimators R-square and adjusted R-square in linear regression. Int J Math Comput 2013;20:85-93.

41. Guo Y, Zhang Z, Zhou B, et al. Grey-matter volume as a potential feature for the classification of alzheimer's disease and mild cognitive impairment: An exploratory study. Neurosci Bull 2014;30:477–89.

42. Luo C, Li M, Qin R, et al. White matter microstructural damage as an early sign of subjective cognitive decline. Front Aging Neurosci 2020;11:1-11

43. Yang C, Zhong S, Zhou X, Wei L, Wang L, Nie S. The abnormality of topological asymmetry between hemispheric brain white matter networks in Alzheimer's disease and mild cognitive impairment. Front Aging Neurosci 2017;9:1–14.

44. Albert MS, DeKosky ST, Dickson D, et al. The diagnosis of mild cognitive impairment due to Alzheimer's disease: recommendations from the national institute on aging-Alzheimer's association workgroups on diagnostic guidelines for Alzheimer's disease. Alzheimers Dement 2011;7:270–9.

45. Amlien IK, Fjell AM. Diffusion tensor imaging of white matter degeneration in Alzheimer's disease and mild cognitive impairment. Neuroscience 2014;276:206–15.

46. Conforti L, Gilley J, Coleman MP. Wallerian degeneration: An emerging axon death pathway linking injury and disease. Nat Rev Neurosci 2014;15:394–409.

47. Zhang M, Zhang J, Zhang W, Yao Z. Demyelination takes place prior to neuronal damage following intracerebroventricular injection of amyloid-beta oligomer. Neuropsychiatry (London) 2018;8:1770–85.

48. Agosta F, Pievani M, Sala S, et al. White matter damage in Alzheimer disease and its relationship to gray matter atrophys. Radiology 2011;258:853–63.

49. Nir TM, Villalon-reina JE, Prasad G, et al. DTI-based maximum density path analysis and classification of Alzheimer's disease. Neurobiol Aging 2015;36:132–40.

50. Chandra A, Dervenoulas G, Politis M. Magnetic resonance imaging in Alzheimer's disease and mild cognitive impairment. J Neurol 2019;266:1293–302.

51. Wang Z, Liang P, Jia X, et al. The baseline and longitudinal changes of PCC connectivity in mild cognitive impairment: A combined structure and resting-state fMRI study. PLoS One 2012;7:1–11.

52. Kompus K, Hugdahl K, Öhman A, Marklund P, Nyberg L. Distinct control networks for cognition and emotion in the prefrontal cortex. Neurosci Lett 2009;467:76–80.

53. Schouten TM, Koini M, De Vos F, et al. Combining anatomical, diffusion, and resting state functional magnetic resonance imaging for individual classification of mild and moderate alzheimer's disease. Neuroimage Clin 2016;11:46–51.

54. Whitwell JL, Dickson DW, Murray ME, et al. Neuroimaging correlates of pathologically-defined atypical Alzheimer's disease. Lancet Neurol 2012;11: 868–77

55. Ioannidis JPA. Why most published research findings are false. PLoS Med 200;2:124.

56. Pereira F, Mitchell T, Botvinick M. Machine learning classifiers and fMRI: a tutorial overview. Neuroimage 2009;45:1–24.

57. Andersson JLR, Skare S, Ashburner J. How to correct susceptibility distortions in spin-echo echo-planar images: application to diffusion tensor imaging. Neuroimage 2003;20:870–88

Voxel-based morphometry results

| ROI | Hemisphere | MNI peak x/y/z | Voxels |
|---|---|---|---|
| | | T-test MCI>AD | |
| PC | L/R | -2 -64 35 | 299 |
| | | T-test HC>AD | |
| ITGP | L/R | 19 42 25 | 4565 |
| Amyg | L | 115 116 62 | 723 |
| Amyg | R | 35 61 30 | 812 |
| Hip | L | 117 100 61 | 1467 |
| Hip | R | 30 53 27 | 1623 |
| Puta | L | 110 132 63 | 749 |
| Puta | R | 35 69 31 | 857 |
| Thala | R | 38 47 39 | 1657 |
| LOCs | L/R | 34 29 66 | 4677 |
| MTGP | L/R | 17 50 31 | 3521 |
| PHA | L/R | 71 124 48 | 2854 |
| PCC | L/R | 46 39 53 | 3816 |
| PC | L/R | 46 32 52 | 4897 |

Table 1: The significant VBM results. The ROIs overlapping with the statistical map are reported, with their peak voxel in MNI coordinates and size of the overlap in voxels. Left (L). Right (R). Inferior Temporal Gyrus posterior (ITGP). Lateral Occipital Cortex superior (LOCs). Middle Temporal Gyrus Posterior (MTGP). Parahippocampal Gyrus Anterior (PHA). Region of interest (ROI). Montreal Neurosciences Institute (MNI). Precuneus cortex (PC). Posterior cingulate cortex (PCC). Alzheimer's disease (AD). Mild cognitive impairment (MCI). Healthy controls (HC). Amygdala (Amyg). Hippocampus (Hip). Thalamus (Thala). Putamen (Puta).

Subcortical segmentation result.

| Subcortical volumen (mm³) | ANCOVA | Post hoc (AD & MCI) | Post hoc (AD & HC) | Post hoc (MCI & HC) |
|---|---|---|---|---|
| L Amygdala | P<0.05* | P>0.05 | 0.0016* | P>0.05 |
| R Amygdala | P>0.05 | - | - | - |
| L Hippocampus | P<0.05* | P>0.05 | 0.0009* | P>0.05 |
| R Hippocampus | P<0.05* | P>0.05 | 0.0012* | P>0.05 |
| L Putamen | P<0.05* | P>0.05 | 0.0021* | P>0.05 |
| R Putamen | P<0.05* | P>0.05 | 0.0018* | P>0.05 |
| R Thalamus | P<0.05* | P>0.05 | 0.0022* | P>0.05 |

Table 2: The subcortical analysis results. The table depicts the results from the one-way analysis of covariance (ANCOVA), age and gender corrected, performed on subcortical structure volumes between the three groups. One asterisk signifies significant difference before, while two asterisks imply significant difference after Bonferroni multiple comparison correction ($p<0.00278$). Left (L). Right (R). Alzheimer's disease (AD). Mild cognitive impairment (MCI). Healthy controls (HC).

Diffusion tensor imaging results

| | ROI | Hemisphere | MNI peak x/y/z | Voxels |
|---|---|---|---|---|
| | | T-test HC>AD (FA) | | |
| A | ACR | L | -22 27 14 | 1184 |
| | ACR | R | 26 25 14 | 1273 |
| | CCB | L/R | -10 -22 30 | 2585 |
| | CCG | L/R | 14 25 16 | 1575 |
| | CCS | L/R | 15 -37 30 | 1855 |
| | EC | L | -30 1 10 | 839 |
| | FM | L/R | -17 37 19 | 5520 |
| | IFOF | L | -32 -72 -1 | 5912 |
| | IFOF | R | 31 -71 6 | 6004 |
| | SLF | L | -42 -50 6 | 7823 |
| | SLF | R | 35 -36 32 | 6816 |
| | | T-test MCI>HC (MD) | | |
| B | CCG | L/R | -9 26 16 | 345 |
| | CCS | L/R | -19 -48 22 | 883 |
| | FM | L/R | -17 35 21 | 2101 |
| | ACR | L | -21 27 4 | 1397 |
| | ACR | R | 18 36 7 | 752 |
| | SCR | L | -22 -5 35 | 1112 |
| | SCR | R | 28 3 26 | 517 |
| | PCR | L | -26 -30 27 | 405 |
| | PCR | R | 26 29 21 | 354 |
| | EC | L | -29 4 10 | 972 |
| | SLF | L | -47 -7 21 | 6510 |
| | IFOF | L | -38 -48 -7 | 5688 |
| | ILF | L | -38 -48 -7 | 3699 |

| | ROI | Hemisphere | MNI peak x/y/z | Voxels |
|---|---|---|---|---|
| | | T-test AD>HC (MD) | | |
| C | CCB | L/R | -9 6 26 | 2547 |
| | CCG | L/R | -7 32 6 | 1665 |
| | CCS | L/R | -16 -47 19 | 2134 |
| | ACR | L | -23 24 19 | 1763 |
| | ACR | R | 25 24 15 | 1702 |
| | SCR | L | -19 -5 40 | 1316 |
| | SCR | R | 24 -3 33 | 1344 |
| | PCR | L | -25 -33 30 | 814 |
| | PCR | R | 24 -37 31 | 873 |
| | EC | L | -22 18 -7 | 1334 |
| | EC | R | 28 14 -4 | 1168 |
| | CH | L | -20 -34 -11 | 302 |
| | CH | R | 22 -30 -12 | 355 |
| | SLF | L | -54 -33 -10 | 13731 |
| | SLF | R | 35 -38 30 | 11743 |
| | ATR | L | -21 27 5 | 9527 |
| | ATR | R | 24 29 16 | 8458 |
| | FM | L/R | -17 40 6 | 8007 |
| | IFOF | L | -22 23 12 | 11571 |
| | IFOF | R | 25 25 16 | 11589 |
| | ILF | L | -30 -55 17 | 8594 |
| | ILF | R | 31 57 4 | 8096 |

| ROI | Hemisphere | MNI peak x/y/z | Voxels |
|---|---|---|---|
| | T-test AD>HC (MD) | | |
| CCB | L/R | -9 6 26 | 2547 |
| CCG | L/R | -7 32 6 | 1665 |
| CCS | L/R | -16 -47 19 | 2134 |
| ACR | L | -23 24 19 | 1763 |
| ACR | R | 25 24 15 | 1702 |
| SCR | L | -19 -5 40 | 1316 |
| SCR | R | 24 -3 33 | 1344 |
| PCR | L | -25 -33 30 | 814 |
| PCR | R | 24 -37 31 | 873 |
| EC | L | -22 18 -7 | 1334 |
| EC | R | 28 14 -4 | 1168 |
| CH | L | -20 -34 -11 | 302 |
| CH | R | 22 -30 -12 | 355 |
| SLF | L | -54 -33 -10 | 13731 |
| SLF | R | 35 -38 30 | 11743 |
| ATR | L | -21 27 5 | 9527 |
| ATR | R | 24 29 16 | 8458 |
| FM | L/R | -17 40 6 | 8007 |
| IFOF | L | -22 23 12 | 11571 |
| IFOF | R | 25 25 16 | 11589 |
| ILF | L | -30 -55 17 | 8594 |
| ILF | R | 31 57 4 | 8096 |

Table 3: The significant diffusion tensor imaging results. Including both fractional anisotropy (FA) measures and mean diffusivity (MD) measures. Additionally, the white matter structures the statistical map overlaps with are displayed, including cluster size (voxels) and peak coordinate (MNI peak x/y/z). Left (L). Right (R). Corpus Callosum body (CCB). Corpus Callosum genu (CCG). Corpus Callosum splenium (CCS). Anterior Corona Radiata (ACR). Superior Corona Radiata (SCR). Posterior Corona Radiata (PCR). External Capsule (EC). Cingulum Hippocampus (CH). Superior Longitudinal Fasciculus (SLF). Anterior Longitudinal Fasciculus (ALF). Anterior Thalamic Radidation (ATR). Forceps Minor (FM). Inferior Fronto-Occipital Fasciculus (IFOF). Inferior Longitudinal Fasciculus (ILF). Region of interest (ROI). Montreal Neurosciences Institute (MNI).

Support vector machine classification

| Groups | Measures | Variables | Final variables | Subjects | VBM/DTI/RS | Accuracy | Sensitivity | Specificity |
|---|---|---|---|---|---|---|---|---|
| MCI vs HC | VBM+DTI+RS | 37 | 14 | 19 | 3/11/0 | 0.67 | 1 | 0.5 |
| MCI vs HC | DTI | 22 | 13 | 19 | 0/13/0 | 0.67 | 1 | 0.5 |
| MCI vs HC | VBM | 14 | 14 | 19 | 14/0/0 | 0.33 | 0.5 | 0 |
| AD vs MCI | VBM+DTI+RS | 37 | 37 | 31 | 14/22/1 | 0.83 | 1 | 0 |
| AD vs MCI | DTI | 22 | 22 | 31 | 0/22/0 | 0.83 | 1 | 0 |
| AD vs MCI | VBM | 14 | 14 | 31 | 14/0/0 | 0.83 | 1 | 0 |
| AD vs HC | VBM+DTI+RS | 37 | 34 | 40 | 13/21/0 | 1 | 1 | 1 |
| AD vs HC | DTI | 22 | 22 | 40 | 0/22/0 | 1 | 1 | 1 |

Table 4: Pairwise classification of the groups. These classifications included single MRI modality and multiple MRI modalities. Voxel-based morphometry (VBM). Diffusion tensor imaging (DTI). Resting state (RS). Alzheimer's disease (AD). Mild cognitive impairment (MCI). Healthy controls (HC).



Multiple linear regression results

~~A~~

| | | MMSE | | |
|---|---|---|---|---|
| Group | subjects | Measures | R | Adjusted $R^2$ |
| AD | 26 | DTI | 0.946 | 0.471 |
| AD | 26 | VBM | 0.913 | 0.654 |
| MCI | 5 | DTI | 0.895 | 0.203 |
| MCI | 5 | VBM | 0.876 | 0.071 |
| HC | 14 | DTI | 0.990 | 0.754 |
| HC | 14 | VBM | 0.992 | 0.798 |

| ~~B~~ | | MoCA | | |
|---|---|---|---|---|
| Group | subjects | Measures | R | Adjusted $R^2$ |
| AD | 26 | DTI | 0.946 | 0.473 |
| AD | 26 | VBM | 0.907 | 0.631 |
| MCI | 5 | DTI | 0.905 | 0.195 |
| MCI | 5 | VBM | 0.855 | 0.087 |
| HC | 14 | DTI | 0.935 | 0.632 |
| HC | 14 | VBM | 0.714 | 0.457 |

Table 5**:** The multiple linear regression results, based on DTI and VBM variables. The table displays the correlation (R) and adjusted $R^2$ value based on Mini mental state examination (MMSE) ~~(panel A)~~ and Montreal cognitive assessment (MoCA) ~~(panel B)~~ score. Voxel-based morphometry (VBM). Diffusion tensor imaging (DTI). Alzheimer’s disease (AD). Mild cognitive impairment (MCI). Healthy controls (HC).

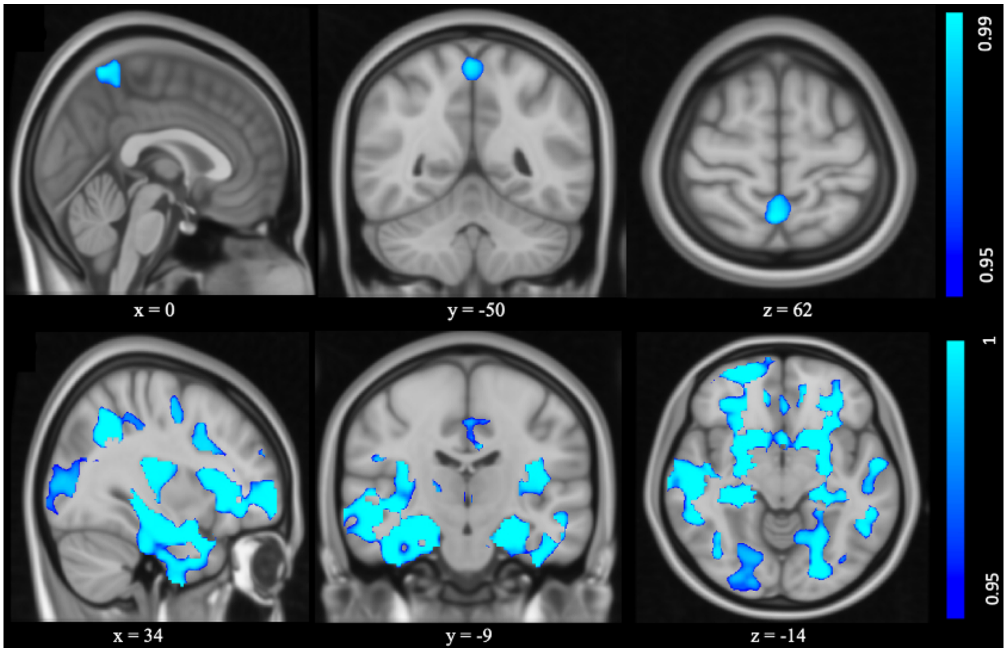


Figure 1: The statistically significant results from the voxel-based morphometry analysis, highlighted in blue on top of the Montreal Neurological Institute-152 1mm template. The top image demonstrates the significant results of t-test Mild cognitive impairment>Alzheimer's disease. The bottom image depicts the significant results from the t-test Healthy control>Alzheimer's disease.

147x95mm (144 x 144 DPI)

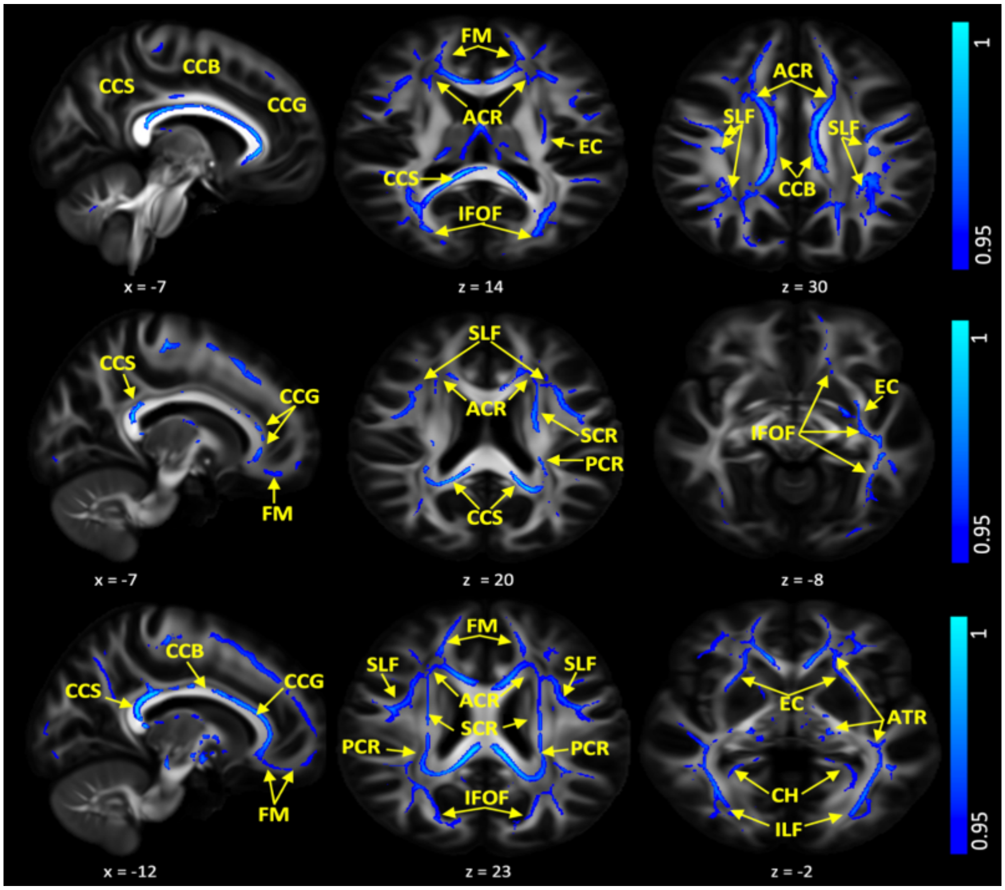


Figure 2: Significant group differences in fractional anisotropy (FA) and mean diffusivity (MD) are highlighted in blue, on top of the FSL_HCP1065_FA_1mm template. The top image illustrates FA difference between healthy controls>Alzheimer's disease, while the middle image exemplifies the difference in MD between mild cognitive impaired>healthy controls. The bottom image demonstrates the MD difference between healthy controls<Alzheimer's disease. Furthermore, the WM tracts overlapping with the statistical map is reported. Corpus Callosum body (CCB). Corpus Callosum genu (CCG). Corpus Callosum splenium (CCS). Anterior Corona Radiata (ACR). Superior Corona Radiata (SCR). External Capsule (EC). Cingulum Hippocampus (CH). Forceps Minor (FM). Inferior Fronto-Occipital Fasciculus (IFOF). Inferior Longitudinal Fasciculus (ILF). Anterior Thalamic Radiation (ATR). Posterior Corona Radiata (PCR).

141x124mm (144 x 144 DPI)